

Broadband visible perfect absorber for sensor based on ultra-thin metamaterial

Xiaoxia Zheng¹ · Zhongyin Xiao¹ · Xinyan Ling¹

Received: 7 October 2016 / Accepted: 25 January 2017 / Published online: 6 February 2017
© Springer Science+Business Media New York 2017

Abstract A metamaterial perfect absorber having a hybrid layer and total thickness of 50 nm is demonstrated in this paper. The results indicate that a broadband absorption above 90% is achieved from 421.2 to 671.8 THz and the absorption of 99.8% can be obtained at the absorption peaks. The absorption is also illustrated to be polarization insensitive under vertical incidence. Furthermore, the broadband and high-efficient absorption are sustained over a wide incident angle range. In addition, the impedance matching theory, surface current distributions, and power loss at the resonant frequencies are also discussed. Moreover, this study demonstrates the application of different permittivity on the performance of the sensor.

1 Introduction

Metamaterials comprised of periodic sub-wavelength structures exhibit unconventional electromagnetic characteristics that cannot be obtained with naturally occurring materials, such as polarization conversion [1], negative refractive [2], and asymmetric transmission [3]. Unit structures such as cut-wire pairs [4], fishnets [5], and metallic split ring resonators [6], have been designed as configuration for metamaterials. Such metamaterials have been desirable to design perfect absorbers [7], sensor [8], light trapping [9] and so on. Actually, metamaterials offer unprecedented properties over a wide range of frequencies throughout microwaves,

terahertz (THz), infrared, and visible regions. In terms of metamaterials, to date investigators have designed a few devices for a variety of applications, including communications [10], energy harvesting [11], imaging [12] and others.

With regard to metamaterial-based absorber, a single frequency perfect absorber was demonstrated by Landy et al. [7]. In addition, some works have been focused on multi-band [13], triple-band [14], and dual-band [15] absorbers which can also realize wide angle incidence, polarization insensitivity within the electromagnetic operation frequencies. However, the bandwidths of the above absorbers hamper their practical application. And expanding their typically limited bandwidth is also our expectation. For example, Yan-Lin Liao and Yao Zhao [16] designed a stacked metal-dielectric grating structure with the same geometrical dimensions in the mid-infrared. The broadband absorption can be realized due to the multi-layer grating enhancing the magnetic field distribution. Zhao et al. [17] presented a metamaterials perfect absorber (MPA) consisting of split ring resonator and lumped resistors from 4.4 to 18 GHz. The relative bandwidth and bandwidth of absorption can achieve 121.4% and 13.6 GHz, respectively.

Recently, few works about perfect absorbers have been put forward to achieve the perfect absorption in visible spectrum. For instance, Lee et al. [18] demonstrated a broadband absorber based on multi-cavity resonances in highly absorbing media in visible range, in which the absorption peak of 95.5% occurs on the resonance frequency. However, the production of the multi-layer structure has the certain difficulty. Rufangura et al. [19] studied a wide-band MPA consisting of concentric circular ring resonator in visible frequency range. The bandwidth of absorption can achieve 33.6 THz. And the disadvantage of this absorber is that the bandwidth is narrow. Thus, a lot

✉ Zhongyin Xiao
zhyxiao@shu.edu.cn

¹ Key Laboratory of Special Fiber Optics and Optical Access Networks, School of Communication and Information Engineering, Shanghai university, Shanghai 200072, China

of efforts are needed to study the perfect MPA in visible region.

In this study, a new ultra-thin absorber is put forward, which is the hybrid material on the top layer. This new design can achieve high absorption for the both transverse electric (TE) and transverse magnetic (TM) waves. In addition, to study the physical mechanism of the absorber we investigate the impedance matching theory, surface current distributions, and power loss at the resonant frequencies. Moreover, the proposed absorber provides an alternative platform to promote potential applications in the areas of solar energy harvesting and sensing. And the effect of the different permittivity on the sensitivity of the sensor is also investigated.

2 Brief theory

The absorption characteristic of the absorber is calculated by $A(\omega) = 1 - R(\omega) - T(\omega)$, where the $A(\omega)$, $T(\omega)$, and $R(\omega)$ represent the absorption, transmittance and reflectance, respectively [19]. The transmittance and reflectance rates depend on the frequency and the S-parameters ($R(\omega) = |S_{11}|^2$, $T(\omega) = |S_{21}|^2$). To achieve maximum absorption rate, the transmittance and reflectance rate should be minimized. So, transmission through the perfect MPA can be completely eliminated using the ground plane. And the absorption rate is then retrieved through $A(\omega) = 1 - R(\omega) = 1 - |S_{11}|^2$ since the transmission is zero.

In addition, the impedance of the MPA structure is expressed as $Z(\omega) = \sqrt{\mu(\omega)/\epsilon(\omega)}$. In order to achieve a perfect absorber, the impedance ($Z(\omega)$) should match to the impedance (Z_0) of vacuum (free space). The transmission and reflection become minimum while the absorption rate reaches its maximum at this matching condition. According to the

basic principle of the impedance match condition to free space, the effective impedance $z = Z(\omega)/Z_0 = 1$, which can be derived by effective medium theory, using the S-parameter retrieval methods. The retrieved impedance z with regard to the S-parameters can be calculated as follows [20]:

$$z = \sqrt{\frac{(1 + S_{11})^2 - S_{21}^2}{(1 - S_{11})^2 - S_{21}^2}} \quad (1)$$

Because the metal plane ground is placed on the bottom for the MPA, $S_{21} = 0$, so the impedance can be expressed as $z = (1 + S_{11})/(1 - S_{11})$. When the real part $\text{Re}(z) = 1$ and the imaginary part $\text{Im}(z) = 0$ of effective wave impedance, the perfect MPA can achieve minimized reflection and transmission, indicating that the perfect absorption.

3 Design and simulation

The configuration of the MPA is depicted in Fig. 1, which is composed of three layers: a hybrid material, a dielectric substrate and a backing sheet. The geometrical parameters are introduced in Table 1. The InSb (red color) and two orthogonal H-shaped structures are placed on the top layer. The H-shaped and the backing sheet are the stannum (Sn) (yellow color) with the thickness of $t = 10$ nm. The top layer and the backing sheet are separated by glass (green color). The relative permittivity and loss tangent of the glass are taken as 4.82 and 0.0054, respectively. The properties of the InSb are described by the simple Drude model [21]:

$$\epsilon(\omega) = \epsilon_\infty - \frac{\omega_p^2}{\omega^2 + i\gamma\omega} \quad (2)$$

$$\omega_p = \sqrt{Ne^2/\epsilon_0 m^*} \quad (3)$$

Fig. 1 The unit cell of the absorber **a** perspective view, **b** bright view, **c** front view

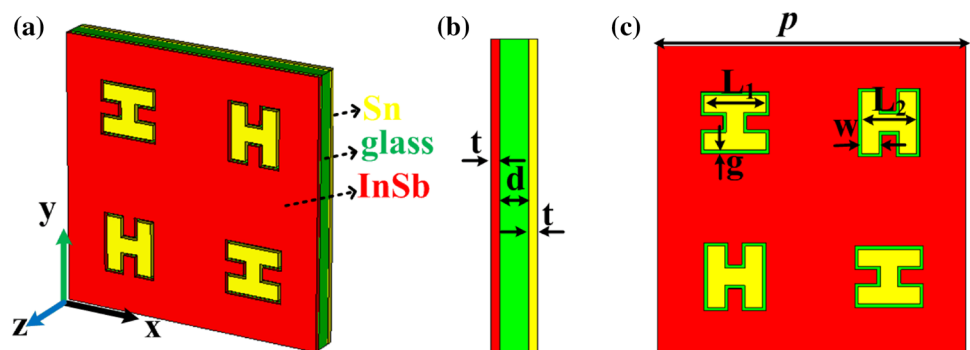


Table 1 Dimensions (in Nanometers) of the Metamaterial Absorber (see Fig. 1)

3D metamaterial	p	d	t	L_1	L_2	w	g
Figure 1b, c	450	30	10	90	80	25	5

In these formulas, ω represents the angular frequency, ϵ_∞ denotes the high-frequency permittivity, γ represents the damping constant, and ω_p is the plasma frequency which rests with the intrinsic carrier density N , the electronic charge e , the vacuum permittivity ϵ_0 , and the effective mass m^* of the carriers. The intrinsic carrier density N (in m^{-3}) of InSb is fit by following formula:

$$N = 5.76 \times 10^{20} T^{1.5} \exp(-0.26/2k_B T) \tag{4}$$

where k_B denotes the Boltzman constant and T represents the kelvin temperature. The numerical simulations are carried out using the full-wave electromagnetic (EM) simulation software (CST Microwave Studio). To calculate the S-parameters, the periodic boundaries and added open space are applied in the x-y plane and z direction as the unit cell conditions, respectively.

The results are present in Fig. 2, which shows that the reflectance, absorption and effective impedance. From Fig. 2a, it can be seen clearly that the absorption is above 90% in the broad frequency from 421.2 to 671.8 THz for both TE and TM polarizations under normal incidence. The results show that the proposed absorber possesses the property of the polarization insensitive. In Fig. 2b, it is worth noting that the real part of the impedance is unity in the vicinity and the imaginary part is close to zero. In other words, this structure was designed so as to be roughly impedance matched ($z=1$) with the bandwidth of 250.6 THz, as this condition is desirable for the perfect absorption. Particularly, around the resonant frequencies of 494.4 and 617.2 THz, the distinct absorption peaks are observed with large absorption efficiency of 99.8 and 99.8% due to the perfect impedance matching condition, respectively.

In fact, the perfect absorption can be enhanced by the hybrid material. From Fig. 3, when the designed structure gets rid of the InSb layer (red line), the highest absorption is 89.6% at frequency of 576.8 THz. When the designed structure removes the four H-shaped resonators (black line), the highest absorption is 68.7% at frequency of 583.2 THz.

Fig. 2 a Simulated reflection and absorption spectra, b calculated real and imaginary of effective impedance under normal incidence

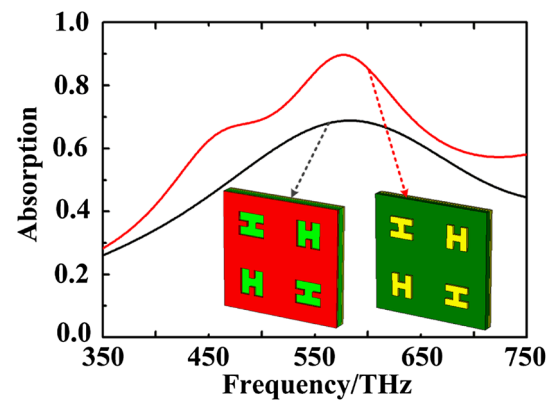
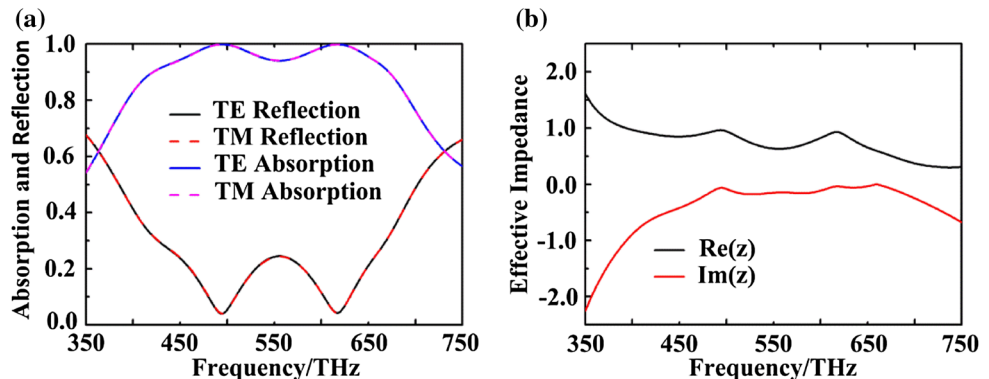


Fig. 3 The absorption of the different absorbers under normal incidence

So, the bandwidth of perfect absorption can be enhanced by using the hybrid material.

The surface current distributions and the power loss density at distinct resonance frequencies are monitored, as shown in Fig. 4. The incident waves can excite circulating currents along the top H-shaped and the bottom layer, thereby giving rise to magnetic dipole moments μ . The resulting magnetic dipoles are parallel. For two magnetic dipoles attraction will lead to an enhanced magnetic interaction shown in Fig. 4a₁ and a₂. In Fig. 4a₁ and a₂, the incident waves can excite the parallel currents between H-shaped and bottom layer, thus the excitation of an electric dipole p exists. For electric dipoles attraction will also result in an enhanced electric interaction [22]. The strong electric and magnetic interactions induce electric and magnetic responses for the case of TE polarization. The electric and magnetic responses result in the induced electric field E and magnetic field H [23]. Furthermore, it indicates that the absorption is induced mainly by the H-shaped resonators at the upper right and lower left corner at low resonance frequency (Fig. 4a₁ and a₂), while the absorption is determined by the four H-shaped resonators at the high resonance frequency

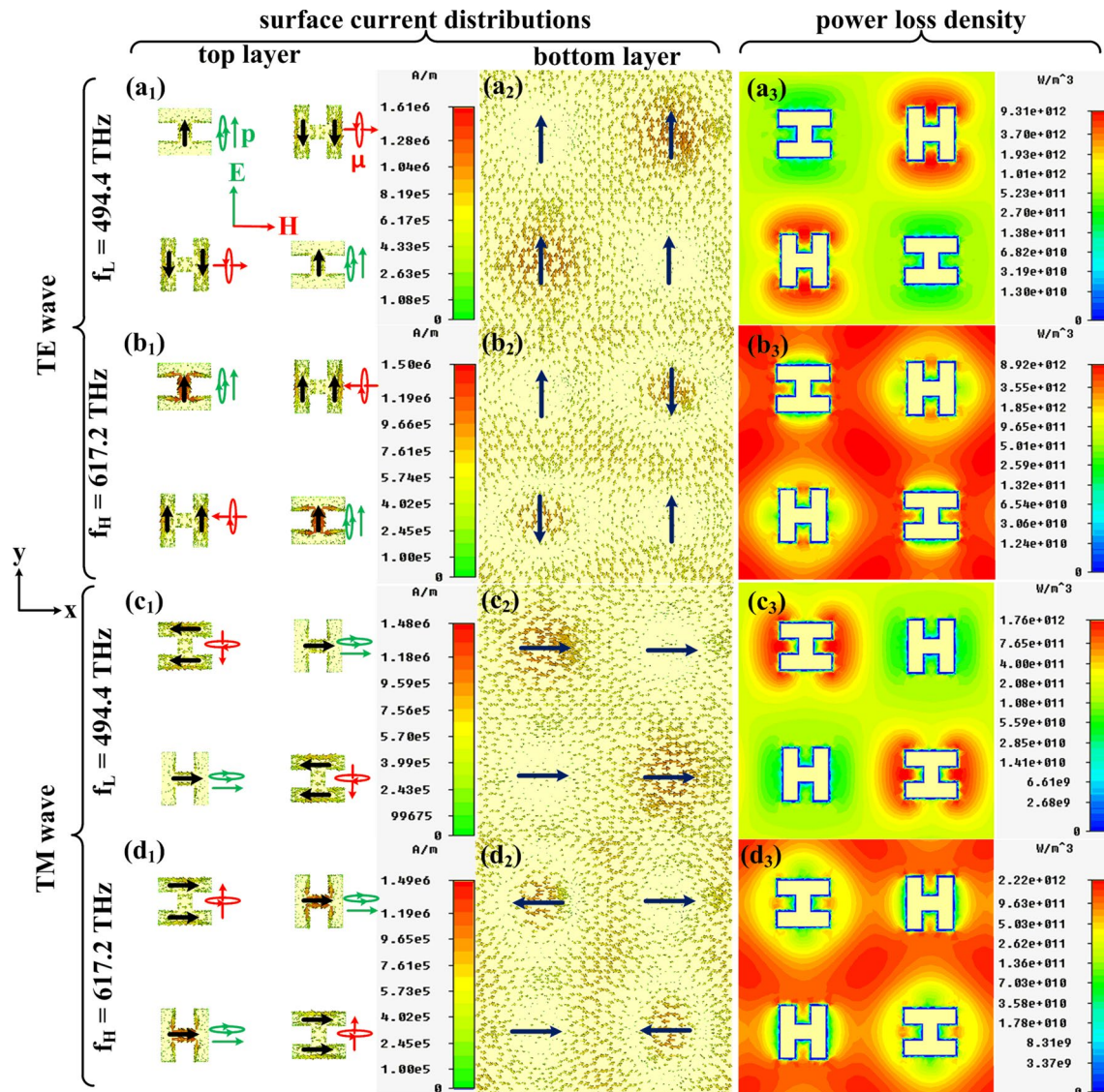


Fig. 4 Surface current distributions and power loss density of the absorber at resonance frequencies

(Fig. 4b₁ and b₂). Therefore, the broadband near perfect absorption can be obtained due to the existence of the resonances. The distributions of power loss density at low and high frequencies are compared in Fig. 4a₃ and b₃, respectively. At the low resonance frequency, the power loss density occurs near the H-shaped resonators at the upper right and lower left corner, with a small portion taking place at the other two H-shaped resonators. At the high resonance frequency, almost all the power loss density appears mainly in the vicinity of the four H-shaped resonators. The strong power loss density reveals the perfect absorption. It is also clear that the distributions of power loss density are similar with the surface current distributions [24]. In addition, the absorption mechanism for TM polarization is similar to the TE polarization.

Based on the above results, the case of TE and TM incident waves impinging on the absorber with different incident angles are also simulated, as presented in Fig. 5a, b, respectively. The incident angle equaling to 0° is the condition that the TE and TM waves are normally incident to the absorber. It illustrates that the broadband and high-efficient absorption are sustained over a wide incident angle range. In Fig. 5a, even though the bandwidth is decreased as the incident angle increases, the absorption over 90% can be obtained from 437.2 to 674.4 THz at the incident angle of 30°. For the case of TM wave, the absorption over 90% can be achieved from 461.2 to 697.2 THz when the incident angle is 45°, as shown in Fig. 5b. However, the position of the lower resonance point (494.4 THz) shifts toward to the low frequency slightly with the increasing of

Fig. 5 Simulated absorption for various angles of incidence **a** TE polarization and **b** TM polarization

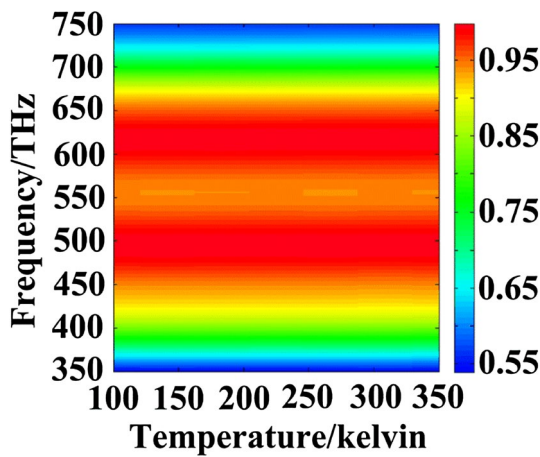
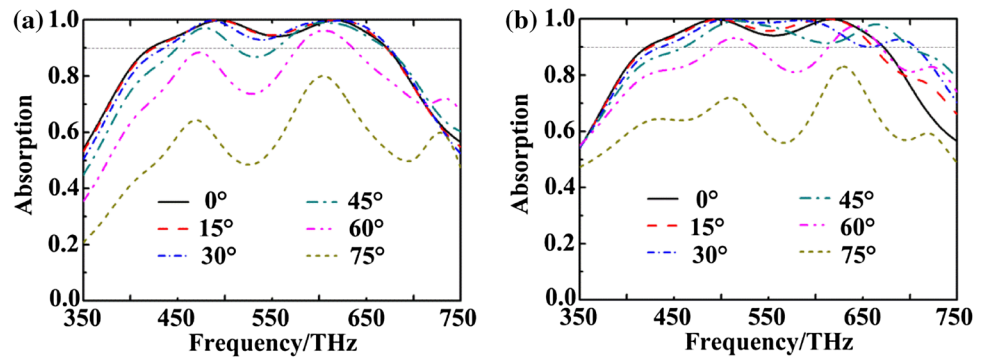


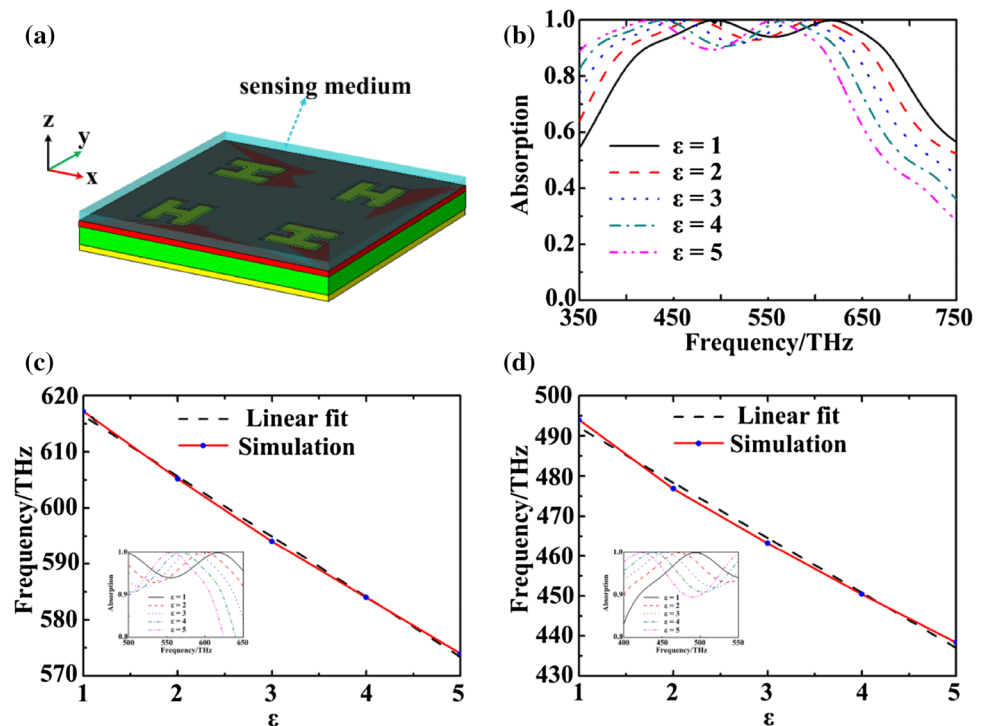
Fig. 6 Absorption of the proposed absorber under different temperature

the incidence angle, especially that for the TE wave. And when the incidence angle changed, the higher frequency point (617.2 THz) will move to the low frequency hardly. Meanwhile, with the increasing of the incidence angle, the lower frequency point has red shift slightly, and the higher resonance point changes obviously.

4 Sensing applications

It is worth mentioning that the permittivity of InSb depends on the temperature. Thus, the permittivity will change with changing of the temperature. However, when the temperature is below 350 K, the damping constant will remain the same. On the other hand, the intrinsic carrier density N will change with changing of the temperature [21]. The

Fig. 7 **a** Varying permittivity layer locate at the top of the designed absorber, **b** resonance shifting of the absorber coated with different permittivity layer, simulated resonance frequencies as a function of permittivity for **c** high resonance frequency, **d** low resonance frequency



absorption under different temperature is shown in Fig. 6. It is more intuitive that the absorption changes with the change of the frequency under the same temperature. However the absorption changes hardly with the various temperatures under the same frequency. Consequently, the absorption can be seen as unchanged when the temperatures change, as this condition is desirable for some applications. In some point of view, the sensing capability of the absorber for the different medium can be observed. Figure 7 depicts the sensing application for different permittivity. Figure 7a shows that a varying permittivity layer with the thickness of 10 nm located at the top of the designed absorber. The simulated variation of the absorption with different permittivity is illustrated in Fig. 7b. It can be obtained that there is a red-shift with the increasing of the permittivity of the sensing medium. Based on Fig. 7b, the relation between the resonant frequencies and the permittivity can be obtained as shown in Fig. 7c, d. From Fig. 7c the red line is the high resonant frequency with different permittivity, while the black line is the linear fitting lines. The red line and the black line are the low resonant frequency with different permittivity and the linear fitting lines in Fig. 7d [25], respectively. It is indicated that the resonance frequencies decrease with the increase of the permittivity, and are sensitivity to the permittivity changing. These results illustrate that the broadband perfect MPA is feasible to work as the permittivity sensor.

5 Conclusions

A new ultra-thin absorber with the hybrid material on the top layer has been demonstrated numerically. The absorption rate is above 90% with the bandwidth of 250.6 THz for both the TE and TM polarizations. Simulated results indicated that the broadband absorber is polarization insensitive under normal incidence and adaptive for a wide range of oblique incident electromagnetic wave. Further study conducted on understanding the physics behind the absorption mechanism of the proposed absorber where impedance matching theory, surface current distributions, and power loss are analyzed. Finally, the sensing capability for different permittivity medium was discussed. And the absorber can be potentially developed as solar energy harvesting.

Acknowledgements This work is supported by the National Natural Science Foundation of China (Grant No. 61275070) and Shanghai Natural Science Foundation (Grant No. 15ZR1415900).

References

1. N.K. Grady, J.E. Heyes, D.R. Chowdhury, Y. Zeng, M.T. Reiten, A.K. Azad, A.J. Taylor, D.A.R. Dalvit, H.T. Chen, *Science* **340**, 1304 (2013)
2. D.R. Smith, J.B. Pendry, M.C. Wiltshire, *Science* **305**, 788 (2004)
3. C. Menzel, C. Helgert, C. Rockstuhl, E.B. Kley, A. Tünnermann, T. Pertsch, F. Lederer, *Phys. Rev. Lett.* **104**, 253902 (2010)
4. Y.J. Yoo, Y.J. Kim, J.S. Hwang, J.Y. Rhee, K.W. Kim, Y.H. Kim, H. Cheong, L.Y. Chen, Y.P. Lee, *Appl. Phys. Lett.* **106**, 071105 (2015)
5. C. Sabah, *J. Mater. Sci.* **27**, 4777 (2016)
6. P. Q. Liu, I. J. Luxmoore, S. A. Mikhailov, N. A. Savostianova, F. Valmorra, J. Faist, G. R. Nash, *Nat. Commun.* **6**, 8969 (2015)
7. N.I. Landy, S. Sajuyigbe, J.J. Mock, D.R. Smith, W.J. Padilla, *Phys. Rev. Lett.* **100**, 207402 (2008)
8. H. Ma, K. Song, L. Zhou, X. Zhao, *Sensors* **15**, 7454 (2015)
9. H. Wang, L. Wang, *AIP Adv.* **5**, 027104 (2015)
10. H. Guo, Z. Sun, J. Sun, N.M. Litchinitser, *IEEE Trans. Antennas Propag.* **63**, 5072 (2015)
11. S. Qi, M. Oudich, Y. Li, B. Assouar, *Appl. Phys. Lett.* **108**, 263501 (2016)
12. C.C. Nadell, C.M. Watts, J.A. Montoya, S. Krishna, W. J. Padilla, *Adv. Opt. Mater.* **4**, 66 (2016)
13. G. Kajtár, M. Kafesaki, E.N. Economou, C.M. Soukoulis, *J. Phys. D* **49**, 055104 (2016)
14. B.X. Wang, G.Z. Wang, T.J. Sang, *J. Phys. D* **49**, 165307 (2016)
15. P. Ruffangura, C. Sabah, *J. Alloys Compd.* **671**, 43 (2016)
16. Y.L. Liao, Y.A. Zhao, *Opt. Commun.* **370**, 245 (2016)
17. J. Zhao, Y. Cheng, *J. Electron. Mater.* **45**, 5033 (2016)
18. K.T. Lee, C. Ji, L.J. Guo, *Appl. Phys. Lett.* **108**, 031107 (2016)
19. P. Ruffangura, C. Sabah, *J. Alloys Compd.* **680**, 473 (2016)
20. D.R. Smith, D.C. Vier, T. Koschny, C.M. Soukoulis, *Phys. Rev. E* **71**, 036617 (2005)
21. H. Liu, G. Ren, Y. Gao, B. Zhu, B. Wu, H. Li, S. Jian, *Plasmonics* **11**, 411 (2016)
22. N. Liu, H. Giessen, *Angew. Chem. Int. Ed.* **49**, 9838 (2010)
23. T.T. Lv, Y.X. Li, H.F. Ma, Z. Zhu, Z.P. Li, C.Y. Guan, J.H. Shi, H. Zhang, T.J. Cui, *Sci. Rep.* **6**, 23186 (2016)
24. Q.Y. Wen, H.W. Zhang, Q.H. Yang, Z. Chen, Y. Long, Y.L. Jing, Y. Lin, P.X. Zhang, *J. Phys. D* **45**, 235106 (2012)
25. Y. Liu, Y. Q. Zhang, X. R. Jin, S. Zhang, Y. P. Lee, *Opt. Commun.* **371**, 173 (2016)